Design of ABC Triblock Copolymers near the ODT with the Random Phase Approximation

Eric W. Cochran, David C. Morse, and Frank S. Bates*

Department of Chemical Engineering and Materials Science, University of Minnesota, Minneapolis, Minnesota 55455-0132

ABSTRACT: Leibler's random phase approximation for block copolymers, modified so as to be applicable to linear multiblock copolymers, has been quantitatively compared to data from three linear ABC/ACB triblock copolymer melts: poly(cyclohexylethylene-*b*-ethylene-*b*-ethylethylene) (CEE$_E$)/CE$_E$E, poly(styrene-*b*-isoprene-*b*-ethylene oxide) (SIO)/ISO (*Macromolecules* **2001**, *34*, 6994−7008; *Macromolecules* **2002**, *35*, 7007−7017), and poly(styrene-*b*-isoprene-*b*-dimethylsiloxane) (SID)/ISD (*Macromolecules* **2002**, *35*, 3189−3197). The RPA calculation provides the mean-field static structure factor for a disordered block copolymer melt, which can be used to anticipate the scattering behavior and spinodal stability limit temperature (T_s); in the context of mean-field theory, the spinodal should lie near the order−disorder-transition temperature (T_{ODT}). We find that the RPA spinodal temperature semiquantitatively matches the magnitude and temperature dependence of the ODT as a function of molecular weight (in CE$_E$E/CEE$_E$) and composition (SIO/ISO). Furthermore, the structure factor also reproduces scattering phenomena in ABC triblock copolymers (ISD/SID) such as the two-peak profile observed in disordered ISD with X-ray scattering. The results show that the RPA is a useful tool in the design of multiblock copolymers without reliance on existing experimental data or cumbersome numerical self-consistent field calculations.

Introduction

ABC triblock copolymers are receiving greater attention[1−13] now that there is a nearly complete understanding of the thermodynamic behavior of the AB diblock copolymer counterparts.[14−17] Part of this attention is focused on the identification of new interesting ordered morphologies, in the hopes of better understanding the governing principles that guide a particular ABC system to a particular morphology. ABCs have great potential for practical applications due to the existence of a wide variety of ABC morphologies that combine the physical properties drawn from three distinct polymers.

Investigating new multiblock copolymer systems presents a daunting task as the phase space to explore is large, and the synthesis and characterization of each new specimen is quite labor intensive. One problem in particular is the location of a suitable molecular weight range over which a new block copolymer species may be studied. The composition $\mathbf{f} = (f_A, f_B, ...)$ and molecular weight of a block copolymer determines the temperature range over which important thermodynamic phenomena exist, most importantly the order−disorder transition temperature (T_{ODT}).

Access to the isotropic state is desirable from both basic research and application-oriented perspectives. From a research perspective, it is useful to have access to the weak and intermediate segregation regimes just below the T_{ODT}, where temperature-dependent morphological transitions and complex ordered phases are known to exist.[16−21] Also, in the disordered state, the system loses its thermal history, facilitating the reformation of structures closer to equilibrium on subsequent cooling. Additionally, the study of morphology alignment under shear or other deformation fields has proven to be most interesting near or even slightly above the T_{ODT}.[12,22−28] From an industrial viewpoint, the state of the melt during processing directly influences production cost (disordered melts are 3−4 orders of magnitude less viscous than their ordered counterparts) and the anisotropy of finished parts.

For any system with a particular set of interaction parameters $\chi_{ij}(T)$, T_{ODT} is purely a function of N, the degree of polymerization, and $\mathbf{f}$. To attain an experimentally accessible T_{ODT} (e.g., between the glass transition or melting temperature and the point of thermal decomposition) at a specimen composition $\mathbf{f}$, N must be within a range determined most often through a resource-intensive process of trial and error. This reliance on empiricism is not due to a lack of theories that successfully describe block copolymer melt thermodynamics. Self-consistent field (SCF) theory can predict the phase behavior of any multiblock copolymer, by calculating the free energies of candidate morphologies for any specified set of values of composition f, statistical segment lengths b_i, binary interaction parameters χ_{ij}, and degree of polymerization N. SCF theory has been used conjointly with experimental data to elucidate the diblock copolymer phase diagram.[14−16] Unfortunately, the spectral implementation of the SCF introduced by Matsen and Schick becomes cumbersome when applied to multiblock copolymers, because it is based on an expansion of composition fields and other basis functions with the space group symmetry of each candidate morphology and thus requires that one be able to anticipate all viable candidate morphologies. A more recent implementation of the SCF theory by Fredrickson and co-workers,[29] and of a closely related density functional theory by Bohbot-Raviv and Wang,[30] promises the ability to predict the preferred morphology, rather than merely compare free energies of candidate structures, by a method analogous to simulated annealing in a simulation cell large enough to contain many unit cells. These methods show great promise in the construction of theoretical phase diagrams for complex polymer melts and mixtures, but like the method of Matsen and Schick, remain too cumbersome to be useful as a tool for

experimentalists in the design of new multiblock copolymers systems.

One of the first theories to successfully predict many of the important features in block copolymer melt thermodynamics was the RPA theory developed by de Gennes[31] for binary homopolymer mixtures, which was later adapted and extended by Leibler[32] to describe weakly segregated homogeneous diblock copolymer melts. Leibler's theory is based on a Landau expansion of the SCF free energy functional in powers of an order parameter

$$\psi(\mathbf{r}) = \langle \delta\rho(\mathbf{r}) \rangle = \langle \rho(\mathbf{r}) - \langle \rho(\mathbf{r}) \rangle \rangle \qquad (1)$$

where $\rho(\mathbf{r})$ is a vector containing the local number density for each component and $\langle...\rangle$ denotes the thermal average. The second-order term in this expansion is proportional to the inverse of the static structure factor of the homogeneous phase, for which Leibler presented explicit expressions. This first result of the original RPA theory is currently the most widely exploited by experimentalists as a fitting function for disordered diblock copolymer scattering data.[33,34] The spinodal (stability) limit of the disordered phase is indicated by the divergence of the structure factor at some critical wavevector of modulus q^*. By considering up to the quartic term in the Landau expansion, Leibler was also able to calculate binodal lines for the classical block copolymer phases (body-centered-cubic spheres, hexagonally packed cylinders, and lamellae) in the weakly segregated regime. As with the spectral implementation of the full SCF theory, evaluation of the phase boundaries required a priori knowledge of the competing phases. However, the calculation of the spinodal limit of the disordered melt requires no such information.

While there are no guarantors that the spinodal conform closely to the equilibrium phase transition, others have nonetheless further adapted the RPA theory for examining the spinodal limits in various block copolymer melts and mixtures.[34−37] For symmetric diblock melts ($f = \frac{1}{2}$, $b_A = b_B$) there is a critical point where binodal and spinodal converge at $\chi N = 10.495$, suggesting that the spinodal temperature limit, T_s, should correspond closely to T_{ODT} near this point in parameter space. However, this point vanishes in higher-dimensional systems. Also, composition fluctuations were predicted by Brazovskii[38] and Frederickson and Helfand[39] to transform the continuous second-order transition predicted by SCF theory to a discontinuous first-order transition at an order−disorder temperature somewhat below the SCF spinodal. While a comparison between the SCF T_s and experimental T_{ODT} is thus not strictly rigorous, any successful correlation of the two quantities lends value to the RPA as a predictive tool.

In this article we use the RPA to model three distinct sets of linear ABC triblock copolymers for both the ABC and ACB topologies: poly(cyclohexylethylene-*b*-ethylene-*b*-ethylethylene) (CEE$_E$) and CE$_E$E, poly(styrene-*b*-isoprene-*b*-ethylene oxide) (SIO) and ISO, and poly-(styrene-*b*-isoprene-*b*-dimethylsiloxane) (SID), and ISD.

In each ABC/ACB system, we probe different aspects of ABC thermodynamics. We have prepared a series of **f** = {0.25,0.50,0.25} CEE$_E$ and CE$_E$E specimens at various molecular weights, totaling 15 compounds. T_{ODT}s were measured by dynamic mechanical analysis (DMA), yielding the function $T_{ODT}(N)$. The SIO and ISO compounds were prepared and rigorously characterized by Bailey et al. in previous studies.[5,40] These were derived from the same symmetric parent SI−OH or IS−OH diblock and vary only in the degree of polymerization of the O block, N_O.

The phase behavior of the SID/ISD systems has recently been reported by Hardy et al.[41] One of the singular traits identified in the ISD sequence was a double-peaked intensity profile in small-angle X-ray scattering (SAXS). This second-order peak was absent using neutrons as the probing radiation and in the homologous compound SID. We make of use of the RPA to explain these phenomena, since the structure factor, the generating function for the intensity profile in all scattering experiments, is directly calculated.

To conduct these analyses, we recast the RPA equation set as presented by Leibler[32] in a matrix formalism that is generally applicable to any block copolymer system, regardless of the number of components or chain architecture. This portion of the work is similar to that done by others.[34−37,42−47] We then present explicit algebraic expressions that may be used to calculate the static structure factor of any linear block copolymer as a function of composition, statistical segment length, and the binary interaction parameters $\chi_{ij}(T)$.

From these comparisons, we demonstrate that the T_s prediction of RPA theory closely matches the order of magnitude and temperature dependence of the T_{ODT} for a variety of real block copolymer systems in addition to accurately representing the isotropic melt structure. This favorable comparison suggests that the theory may be useful as a tool in designing the appropriate molecular weight range for the study of any block copolymer system with experimentally accessible T_{ODT} values.

Experimental Section

Precursor Synthesis. The materials used in this study were all prepared by sequential anionic polymerization of styrene and butadiene to yield unsaturated block copolymer precursors, which subsequently were saturated by heterogeneous catalytic hydrogenation to yield the desired block copolymer. Poly(styrene) (S) is the precursor to poly(cyclohexylethylene), 1,4-poly(butadiene) (B$_{14}$) is the precursor to poly(ethylene), and 1,2-poly(butadiene) (B$_{12}$) is the precursor to poly(ethylethylene).

All monomers and solvents were purified rigorously before polymerization according to techniques described elsewhere.[48] Polymerization was initiated by addition of *sec*-butyllithium to cyclohexane at 40 °C under 3 psig of argon. The active initiator concentration was ascertained by Gilman double-titration.[49] The reaction sequence began with the addition of the first monomer, butadiene or styrene. Under these conditions, butadiene is known to favor 93% 1,4 addition.[50] After 8 h, a small aliquot was cannulated from the reactor and terminated with degassed methanol for molecular weight distribution analysis using size exclusion chromatography (SEC). For SB$_{14}$B$_{12}$, the second block addition occurred under identical conditions. Prior to the initiation of the B$_{12}$ block, the reaction medium was cooled to 10 °C and a 100:1 molar ratio of THF was added. Such conditions accelerate the polymerization of both the S and B blocks[21] and cause the butadiene to favor 90% 1,2 addition.[50] Under these conditions both the B$_{12}$ and S polymerization reactions were maintained for at least 4 h, to attain >99% conversion. Following the completion of the final block, the active chains were terminated with degassed methanol.

Recovery of all unsaturated precursors was achieved through precipitation at room temperature into a 3:1 mixture of methanol and 2-propanol, followed by drying under dynamic vacuum to constant mass.

Heterogeneous Catalytic Saturation. Saturated polymers were obtained by hydrogenation of the precursor materials. These reactions were conducted in an agitated stainless

Table 1. Polymer Physical Property Data at 140 °C

	Chemical Structure	M_0, Da	$\dfrac{M}{N}$[a] Da	ρ, $\dfrac{g}{cm^3}$[b]	b, Å[c]	ρ_e[d], $\dfrac{mol\ e^-}{cm^3}$	$\left(\dfrac{b}{v}\right)^e \times 10^{10}$, cm^{-2}
C		109	65.4	0.92	4.60	0.515	0.233
E[f]		28	55.8	0.78	8.35	0.448	-0.280
E_E[f]		56	57.4	0.81	5.39	0.461	-0.288
S		104	56.2	0.97	5.47	0.522	1.306
I		68	59.0	0.83	6.07	0.464	0.245
O		44	75.6	1.06	7.80	0.580	0.603
D		74	63.6	0.895	5.39	0.484	0.059

[a] Molar mass of a statistical segment, corresponding to a 118 Å^3 reference volume. [b] Mass density.[55] [c] Statistical segment length with respect to reference volume.[55] [d] Electron density, proportional to the scattering power for X-rays. [e] Neutron scattering cross-section density, where b is the coherent scattering length per monomer and v is the monomer volume. [f] E and E_E contain 2 and 40.9 ethyl branches per 100 backbone carbons.

steel pressure vessel described elsewhere.[51] A typical saturation reaction consisted of dissolving 5 g of precursor into 500 mL of cyclohexane followed by intense mixing with 0.5 g of a 5% Pt/SiO$_2$ catalyst[51-54] for 12 h at 170 °C under 500 psi of H$_2$. The product materials were recovered by precipitation into a 6:1 mixture of methanol and 2-propanol and dried to constant mass under dynamic vacuum.

Molecular Characterization. Compositions of all materials were determined from integrated ^{1}H NMR spectra collected on the unsaturated precursor polymers dissolved in deuterated chloroform with a 300 MHz Varian instrument operating at room temperature. Mole fractions of S, B_{14}, and B_{12} were converted to volume fractions C, E, and E_E using reported densities at 140 °C (see Table 1).[55] ^{1}H NMR also was used to establish the level of saturation in the products. CE$_E$E and CEE$_E$ spectra were obtained at room temperature and 50 °C, respectively; the elevated temperature was required to completely dissolve CEE$_E$ in chloroform. Over 99% saturation was achieved in all the materials discussed here.

Molecular weights were calculated for all CEE$_E$ specimens using M_n of the S block (from the aliquot taken during synthesis) as measured with PS-calibrated SEC traces and the mass fraction of the S block as determined by NMR. SEC also was used to compute the polydispersity of all precursor materials with respect to PS standards, which in every case was less than or equal to 1.04, and to confirm that the saturation process did not lead to any degradation of the molecular weight distribution.

High-performance size exclusion chromatography (HPSEC) was used to measure the molecular weight of SB$_{12}$B$_{14}$ specimens using Phenonmenex Phenolgel columns coupled to a Wyatt Dawn DSP laser photometer using detectors at 18 angles and a Wyatt differential refractometer. THF was the mobile phase. CE$_E$E molecular weights were computed from the known composition and molecular weights of the SB$_{12}$B$_{14}$ precursors.

Dynamic Mechanical Analysis. Order–disorder phase transitions were identified through dynamic mechanical spectroscopy (DMS) measurements conducted with a Rheometrics Scientific ARES strain-controlled rheometer fitted with 25 mm parallel plates. Samples were prepared by compression molding into 25 mm × 1 mm disks for 5–10 min at 500 psi and 160 °C, which is well above the $T_{g,C}$, the highest thermal transition in the system. Samples were heated under nitrogen in the rheometer to roughly 10 °C above T_{ODT} to erase any thermal history in the materials, and then cooled to 135 °C prior to beginning the isochronal temperature ramp experiment. The strain amplitude was initially set to 1%, but was automatically increased to as high as 5% as necessary to maintain a sufficient torque signal. This limit was chosen so that all measurements were taken within the linear viscoelastic regime. The frequency was in all but two instances 1 rad/s, corresponding to $\omega < \omega_c$, where ω_c represents the crossover frequency separating domain and single-chain dynamics.[56,57] For CEE$_E$-2 and CEE$_E$-3, 1 rad/s > ω_c, as determined by isothermal frequency scans, and thus in order to detect T_{ODT}, ω was reduced to 0.1 rad/s.

Small-Angle X-ray Scattering (SAXS). SAXS experiments were conducted at the University of Minnesota Institute of Technology characterization facility. Copper Kα radiation (wavelength $\lambda = 1.54$ Å) was supplied by a Ragaku Ru-200BVH rotating anode using a 0.2 × 2.0 mm^2 microfocus cathode with monochromatization by total reflecting Franks mirrors and a nickel foil filter. Samples were placed in an evacuated sample chamber. Temperature was controlled by two resistive elements connected to a water-cooled brass sample holder. Two-dimensional data were collected with a Siemens HI–STAR multiwire area detector and were corrected for detector response characteristics. These were converted to the conventional intensity I vs wavevector **q** form via azimuthal integration and the relationship $q = |\mathbf{q}| = (4\pi/\lambda)\sin(\theta/2)$, where θ is the scattering angle.

The Random Phase Approximation (RPA) for a Linear Multiblock Copolymer

We wish to obtain expressions from which the static structure factor for a disordered asymmetric multiblock copolymer may be directly evaluated. We restrict our analysis to the case of a monodisperse, incompressible, amorphous, n-block copolymer melt. Our derivation is closely related to several prior treatments.[34-37,42-47] Each block i is characterized by its volume fraction $f_i = N_i/N$ and statistical segment length b_i, where N_i is the number of statistical segments for block i, and N is the total number of segments in a chain. The interaction strength between blocks i and j is represented by $\chi_{ij}(T)$, which is located in the ith row and jth column of the symmetric matrix $\chi(T)$. We consider an incompressible melt, and define statistical segments for each species so as to occupy a reference volume v_0, which is the same for all species. This yields a statistical segment for species i of molecular weight $m_i = N_A\rho_i v_0$, where ρ_i is the mass density of a melt of homopolymer i and N_A is Avogadro's number, and statistical segment length $b_i^2 = m_i 6(R_g^2/M)_i$, where $(R_g^2/M)_i$ is the ratio of radius of

gyration to molecular weight in a hompolymer melt of species *i*.

Define the column vector $\rho(\mathbf{r})$

$$\rho(\mathbf{r}) = \begin{pmatrix} \rho_1(\mathbf{r}) \\ \vdots \\ \rho_n(\mathbf{r}) \end{pmatrix} \tag{2}$$

whose elements are dimensionless number densities of each component at location $\mathbf{r}$, such that $\rho_i(\mathbf{r}) \equiv v_0 c_i(\mathbf{r})$, where $c_i(\mathbf{r})$ is the local number density of statistical segments of species *i*. In the disordered state, $\langle \rho_i(\mathbf{r}) \rangle = f_i$, where $\langle ... \rangle$ denotes the thermal average.

Now define an order parameter

$$\psi(\mathbf{r}) = \langle \rho(\mathbf{r}) - \langle \rho(\mathbf{r}) \rangle \rangle \tag{3}$$

that vanishes in the disordered phase and varies periodically in an ordered phase. Following Leibler,[32] the analysis begins by evaluating the linear response of $\psi(\mathbf{r})$ to a fictitious external potential $\mu^{\text{ext}}(\mathbf{r})$, a column vector whose *i*th component is the chemical potential field subject to monomers of type *i*. For a noninteracting ideal gas of block copolymer chains there exists a response function $\underline{\mathbf{R}}(\mathbf{r} - \mathbf{r}')$ such that

$$\psi(\mathbf{r}) = -\int d\mathbf{r}' \underline{\mathbf{R}}(\mathbf{r} - \mathbf{r}') \mu^{\text{ext}}(\mathbf{r})' \tag{4}$$

A more convenient representation is in the Fourier domain

$$\psi(\mathbf{q}) = \underline{\mathbf{R}}(\mathbf{q}) \mu^{\text{ext}}(\mathbf{q}) \tag{5}$$

We may now take into account interactions between polymers at a mean-field level by replacing μ^{ext} with an effective field μ^{eff} in eq 5, taking $\psi(\mathbf{q}) = \underline{\mathbf{R}}(\mathbf{q}) \mu^{\text{eff}}(\mathbf{q})$, where

$$\mu^{\text{eff}}(\mathbf{q}) = \mu^{\text{ext}}(\mathbf{q}) + k_B T \chi(T) \psi(\mathbf{q}, T) + \mathbf{F} \tag{6}$$

Here, k_B is Boltzmann's constant, $k_B T \chi(T) \psi(\mathbf{q})$ is the interaction potential, and $\mathbf{F}$ is a Lagrange multiplier (pressure) field that enforces compressibility. The form of $\mathbf{F}$ is $\lambda \epsilon$, where ϵ is an *n*-dimensional column vector of 1's and λ is a scalar quantity determined by invoking the constraint of incompressibility

$$\sum_{i=1}^{n} \langle \delta \rho \rangle_i = \epsilon^t \psi = 0 = \epsilon^t \underline{\mathbf{R}} \mu^{\text{ext}} + k_B T \epsilon^t \underline{\mathbf{R}} \chi(T) \psi + \lambda \epsilon^t \underline{\mathbf{R}} \, \epsilon \tag{7}$$

Solving

$$\lambda = -\frac{\epsilon^t \underline{\mathbf{R}}(\mu^{\text{ext}} + k_B T \chi(T) \rho)}{\epsilon^t \underline{\mathbf{R}} \epsilon} \tag{8}$$

Inserting (8) into (6) yields

$$\psi(\mathbf{q}, T) = -(\underline{\mathbf{I}} + k_B T \tilde{\underline{\mathbf{R}}}^0(\mathbf{q}) \chi(T))^{-1} \tilde{\underline{\mathbf{R}}}^0(\mathbf{q}) \mu^{\text{ext}}(\mathbf{q}) \tag{9}$$

where $\underline{\mathbf{I}}$ is the identity and $\tilde{\underline{\mathbf{R}}}^0(\mathbf{q}) = \underline{\mathbf{R}}(\mathbf{q})(\mathbf{I} - (\epsilon \epsilon^t \underline{\mathbf{R}}(\mathbf{q}))/(\epsilon^t \underline{\mathbf{R}}(\mathbf{q}) \epsilon)$, the response function of an incompressible melt when $\chi_{ij} = 0$. From (9), it is apparent that the corrected response function is

$$\tilde{\underline{\mathbf{R}}}(\mathbf{q}, T) = (\tilde{\underline{\mathbf{R}}}^0(\mathbf{q})^{-1} + k_B T \chi(T))^{-1} \tag{10}$$

The fluctuation−dissipation theorem relates the response function to the structure factor:

$$\underline{\mathbf{S}}(\mathbf{q}, T) = k_B T \underline{\mathbf{R}}(\mathbf{q}, T) \tag{11}$$

This relationship holds for both the response function $\mathbf{R}(\mathbf{q})$ of the hypothetical ideal gas and for the response $\tilde{\mathbf{R}}^0(\mathbf{q})$ of the interacting melt and so allows us to rewrite eq 10 for the response function as an expression for the structure factor:

$$\tilde{\underline{\mathbf{S}}}(\mathbf{q}, T) = (\tilde{\underline{\mathbf{S}}}^0(\mathbf{q})^{-1} + \chi(T))^{-1} \tag{12}$$

We wish to study specifically asymmetric, linear ABC triblock copolymers. All that needs to be specified is the ideal gas pair correlation matrix $\underline{\mathbf{S}}(\mathbf{q}) = k_B T \underline{\mathbf{R}}(\mathbf{q})$. The correlation function for a noninteracting Gaussian homopolymer given by the integral

$$S(q) = \frac{N}{v_0} \int_0^1 \int_0^1 e^{-q^2 \left(N b^2/6\right)|x - x'|} \, dx \, dx' \tag{13}$$

which yields a Debye function. To extend this function to the case of a multiblock copolymer we must consider the $n(n + 1)/2$ separate correlation functions between each block *i* with block *j*. These correlation functions are analogous to that for the homopolymer chain. To determine them, first define the beginning of block *i* as $x_i = \sum_{j=1}^{i-1} f_j$ and its termination as $x_{i+1} = \sum_{j=1}^{i} f_j$. Then the elements of the ideal gas correlation matrix for a linear multiblock copolymer are

$$S_{ii}(q) = \frac{N}{v_0} \int_{x_i}^{x_{i+1}} \int_{x_i}^{x_{i+1}} e^{-q^2(N b_i^2/6)|x-x'|} \, dx \, dx' \tag{14}$$

$$= \frac{N}{v_0} \frac{2}{q^2 \frac{N_i b_i^2}{6}} \left(e^{-f_i q^2 \left(N_i b_i^2/6\right)} + f_i q^2 \frac{N_i b_i^2}{6} - 1 \right)$$

for $i = j$, and

$$S_{ij} = \frac{N}{v_0} \int_{x_i}^{x_{i+1}} \int_{x_j}^{x_{j+1}} e^{-q^2 N((x_{i+1}-x)b_i^2 + \sum_{k=i+1}^{j-1} f_k b_k^2 + (x'-x_j)b_j^2)} \, dx \, dx' \tag{15}$$

$$= \frac{N}{v_0} \frac{36 e^{(-q^2)/(6) N \sum_{k=i+1}^{j-1} f_k b_k^2}}{N b_i^2 N b_j^2 q^4} ((1 - e^{-q^2 (N b_i^2/6) f_i}) \times$$

$$(1 - e^{-q^2 (N b_j^2/6) f_j}))$$

for $i \neq j$. For the diblock case, these functions reduce to the 2×2 matrix form published by Leibler.

We note that while in diblock copolymers the segregation strength may be described by a single dimensionless parameter χN, there is no such scalar analogue in multicomponent systems. This fact makes a universal description of important thermodynamic features in the multiblock copolymer phase diagrams intractable. For instance, the spinodal limit in symmetric diblock copolymers occurs for $\chi N = 10.495$. However, in multiblock copolymers there is no unique value of χN_{ODT} for any specific composition. Without further constraining the relationships of the interaction parameters with
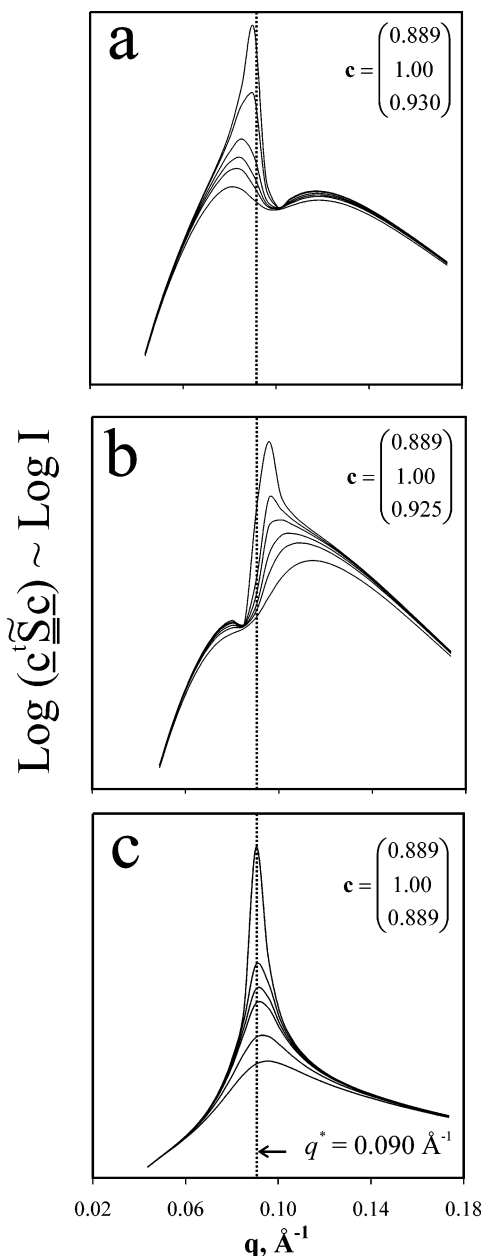
Figure 1. Computed RPA scattering of a model compositionally symmetric, $N = 100$ ISD block copolymer, at six temperatures approaching the spinodal limit for three different choices of the scattering contrast vector **c**. The temperatures shown in each instance are $1.0324 T_s$, $1.0171 T_s$, $1.0121 T_s$, $1.0072 T_s$, $1.0020 T_s$, and $1.0002 T_s$, where $T_s = 302.4$ K. Temperature decreases with increasing peak intensity.

each other the only scalar variable that can uniquely locate the spinodal point is the temperature T_s.

As the disordered melt is cooled toward T_s, density fluctuations increase without bound as the result of the divergence at $T = T_s$ of one of the eigenvalues of the matrix $\underline{\tilde{\mathbf{S}}}(q)$ at some critical wavenumber $q = q^*$. In addition to predicting the spinodal limit, the RPA/mean-field theory structure factor presented in eq 12 may also be used to predict the scattering intensity profile $I(q)$ for any type of radiation using

$$I(q) = \mathbf{c}^t \underline{\tilde{\mathbf{S}}} \mathbf{c} \tag{16}$$

where **c** contains the appropriate scattering densities, or contrast factors, for each monomer type. The n-dimensional structure factor matrix is symmetric, where

the diagonal elements are given by

$$\underline{\tilde{\mathbf{S}}}_{ii} = -\sum_{j, i \neq j}^{n} \underline{\tilde{\mathbf{S}}}_{ij} \tag{17}$$

as a result of the constraint of incompressibility. Substitution of eq 17 into eq 16 leads to the following form for $I(q)$ in a disordered n-block copolymer:

$$I(q) = -\sum_{i=2}^{n} \sum_{j=1}^{i-1} (c_i - c_j)^2 \underline{\tilde{\mathbf{S}}}_{ij} \tag{18}$$

For a diblock, $S_{11} = S_{22} = -S_{12} = -S_{21}$, and we recover Leibler's result

$$I(q) = (c_1 - c_2)^2 \frac{W(q)}{S(q) - 2\chi W(q)} \tag{19}$$

where $W(q)$ is the determinant and $S(q)$ is the sum of the elements of the ideal gas correlation matrix calculated using eqs 14 and 15.

The divergence of the scattering intensity for multiblock copolymers signals the stability limit much in the same way as in diblock copolymers, although its complexity can be considerably greater due to the addition of block topology as a variable and the introduction of additional competing interaction parameters. The structure factor of an ABC triblock copolymer contains correlation information about the A/B, A/C, and B/C length scales. When these length scales differ sufficiently, there is a potential for scattering experiments to differentiate them. Different scattering experiments show the six monomer−monomer correlations with different weights, and thus the scattering behavior of a single species can be markedly different depending on the type of probing radiation. However, as the disordered melt reaches the spinodal, the divergent eigenmode of the structure factor always begins to dominate the scattering at a unique value of q^*, regardless of the type of radiation.

Figure 1 demonstrates this point by plotting the computed intensity for a model, compositionally symmetric ISD triblock copolymer ($N = 100$), using the statistical segment lengths tabulated in Table 1 and the interaction parameters in Table 3 at various temperatures approaching the spinodal limit ($T_s = 302.4$ K in this example). We show three cases with different choices for the scattering contrast vector **c**. In each case the scattered intensity profile is distinct, since the relative values of **c** determine which of the correlations in the structure factor are most pronounced. The first two cases (Figure 1, parts a and b) show a double-peaked profile, which is unknown in diblock copolymers but is consistent with the existence of multiple length scales in multiblock copolymers. In the first case, the lowest angle peak is dominant and grows as the temperature is reduced until it diverges, while in the second case it is the second peak that is dominant. In the third case (Figure 1c), two of the scattering densities have been set equal, which completely obscures the existence of multiple length scales and yields a single peak. In all three cases, however, the scattering diverges at the same value of $q^* = 0.090$ Å^{-1}.

$T_{ODT}(M_n)$ Characterization for CE$_E$E and CEE$_E$ Triblocks

Characterization data for all specimens used in this study appear in Table 2. The number-average polym-

Table 2. Characterization Data for Triblock Copolymers

polymer	M_n	M_w/M_n	N_n	f_A	f_B	f_C	$T_{ODT},$ °C
(a) CEE$_E$/CE$_E$E Triblock Copolymers							
CE$_E$E-1	25 390	1.04	452	0.20	0.54	0.26	145
CE$_E$E-2	26 750	1.02	473	0.26	0.51	0.23	174
CE$_E$E-3	30 500	1.08	539	0.26	0.50	0.24	180
CE$_E$E-4	29 610	1.03	523	0.27	0.44	0.29	222
CE$_E$E-5	37 510	1.02	663	0.26	0.50	0.24	267
CE$_E$E-6	41 090	1.01	726	0.26	0.50	0.24	280
CE$_E$E-7	64 590	1.01	1141	0.26	0.50	0.24	>300
CEE$_E$-1	22 841	1.02	388	0.26	0.48	0.26	<135
CEE$_E$-2	26 115	1.02	443	0.27	0.49	0.24	172
CEE$_E$-3	29 501	1.02	501	0.27	0.47	0.26	172
CEE$_E$-4	33 561	1.02	570	0.27	0.47	0.26	220
CEE$_E$-5	34 292	1.02	584	0.26	0.48	0.26	217
CEE$_E$-6	37 735	1.03	642	0.26	0.46	0.27	243
CEE$_E$-7	42 433	1.02	722	0.26	0.47	0.27	287
CEE$_E$-8	44 668	1.03	759	0.27	0.47	0.26	328
(b) SIO/ISO Triblock Copolymers[5,40]							
SI-OH	18 760	1.04	293	0.50	0.50	0.00	115
SIO blend DB/A-1	19 054		297	0.49	0.49	0.02	95
SIO A	19 370	1.08	302	0.48	0.49	0.03	84
SIO blend A/B-1	19 722		306	0.48	0.48	0.04	90
SIO blend A/B-2	20 098		311	0.47	0.47	0.06	100
SIO B	20 450	1.07	316	0.46	0.47	0.07	112
SIO C	20 530	1.07	317	0.46	0.46	0.08	118
SIO blend C/D-1	20 799		320	0.46	0.46	0.09	130
SIO blend C/D-2	21 094		324	0.45	0.45	0.10	145
SIO D	21 390	1.08	328	0.44	0.45	0.11	153
SIO E	21 960	1.09	336	0.43	0.44	0.13	164
SIO F	23 110	1.11	351	0.42	0.42	0.17	191
SIO blend F/G-I	23 589		357	0.41	0.41	0.18	205
SIO blend F/G-2	24 101		364	0.40	0.40	0.20	210
G	24 580	1.1	370	0.39	0.40	0.21	216
SIO blend G/H-1	24 901		375	0.39	0.39	0.22	225
H	25 580	1.11	384	0.38	0.38	0.27	>225
IS-OH3	13 550	1.05	212	0.50	0.50	0.00	97
ISO1	13 810	1.05	215	0.49	0.49	0.02	111
ISO2	14 330	1.05	222	0.48	0.47	0.05	134
ISO3	14 610	1.05	226	0.47	0.47	0.07	146
ISO4	15 240	1.05	234	0.45	0.45	0.10	164
ISO5	15 780	1.05	241	0.44	0.44	0.13	194
ISO6	16 320	1.05	249	0.43	0.42	0.15	217
ISO7	16 930	1.05	257	0.41	0.41	0.18	246
ISO8	17 080	1.05	259	0.41	0.41	0.18	251
ISO9	17 780	1.05	268	0.40	0.39	0.21	267
ISO10	18 520	1.05	278	0.38	0.38	0.24	293
ISO11	19 440	1.05	290	0.37	0.36	0.27	302
ISO12	20 380	1.05	302	0.35	0.35	0.30	307
ISO13	21 770	1.05	321	0.33	0.33	0.34	310
(c) SID/ISD Triblock Copolymers[41]							
SID7	8500	1.14	293	0.33	0.32	0.35	227
ISD4	12 300	1.06	297	0.36	0.38	0.26	165

Table 3. Correlations of the Form $\chi_{AB} = A/T + B$ for the Flory Interaction Parameter

binary pair[a]	A, K	$B \times 10^3$
CE	29.4	−17.4
CE$_E$	11.2	−8.7
CP	15.7	−3.6
E$_E$E	12.0	−4.5
E$_E$P	4.9	−0.5
EP	8.9	−16.2
SI	26.4	−2.9
SD	68.0	37
SO	29.8	−22.9
ID	43.6	−10
IO	90.0	−57.9

[a] CE, CE$_E$, and CP from ref 64. E$_E$E and E$_E$P from ref 63, EP from ref 33, SI from ref 65, and SD, SO, ID, and IO from ref 66.
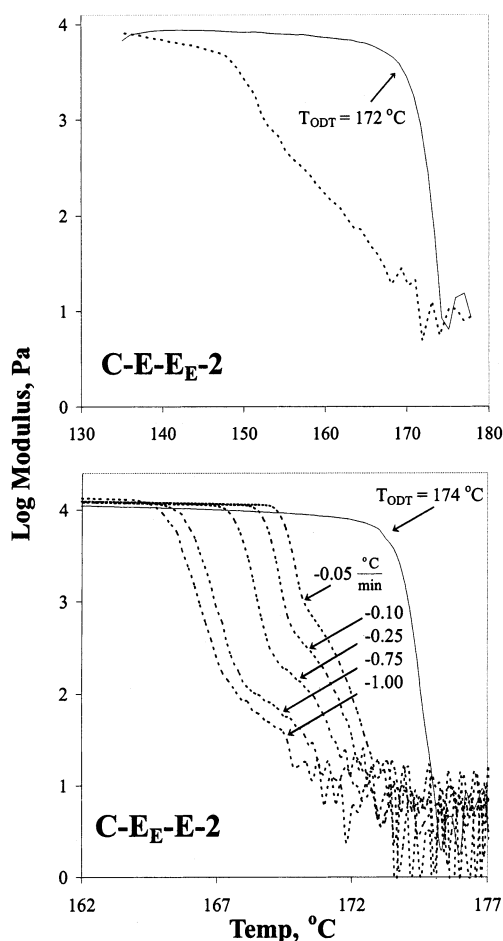

Figure 2. $G'(T)$ for CEE$_E$-2 and CE$_E$E-2 for heating and cooling. The frequency was 1 rad/s for CE$_E$E and 0.25 rad/s for CEE$_E$. The heating and cooling rate was 1 °C/min for CEE$_E$. The heating rate for CE$_E$E was 1 °C/min as well, although the cooling experiment was conducted at a variety of rates ranging from 0.05 to 1 °C/min.

erization index N_n is based on a common segment reference volume of $v_0 = 118$ Å^3, corresponding roughly to the volume of a four-carbon repeat unit.

Low frequency ($\omega < \omega_c$) isochronal DMS measurements, an established technique for detecting phase transitions in block copolymer melts,[56−58] were used to obtain the T_{ODT} values reported in Table 2 for CEE$_E$ and CE$_E$E specimens. We provide representative $G'(T)$ traces obtained while heating and cooling (1 °C/min) for CEE$_E$-2 and CE$_E$E-2 in Figure 2. The order−disorder transition is marked by the precipitous 3−4 order of magnitude decrease in the elastic modulus during heating. The temperature of this transition is not rate-dependent for slow heating rates (i.e., 1 °C/min). However the reordering transition on cooling, which usually occurs through classical nucleation and growth,[59−62] is strongly rate-dependent. This rate dependence is demonstrated for CE$_E$E-2 in Figure 2 by the various dashed

curves that show $G'(T)$ during reordering at cooling rates varying from 0.05 to 1 °C/min. Depending on cooling rate, reordering occurs over time scales ranging from minutes to hours. Regardless of cooling rate, there are three distinct kinetic regimes evident from the discontinuities in the derivative of $G'(T)$: an initial rapid increase from the disordered state, followed by a slower ordering process, which then reverts to an accelerated process that persists until the specimen is fully ordered. Since this behavior is independent of cooling rate, the rapid reordering at deep quenches (large cooling rate)
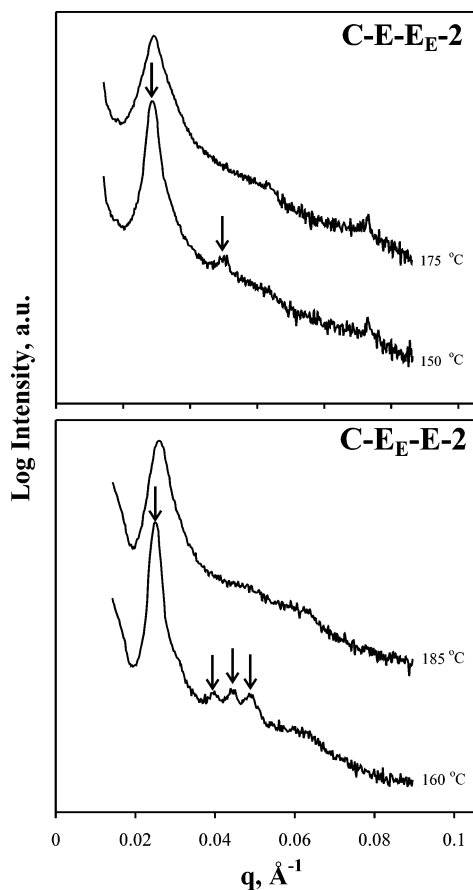
Figure 3. Azimuthally integrated $I(q)$ SAXS data for CEE_E-2 and CE_EE-2 in the ordered and disordered phases. Both species clearly exhibit multiple orders of Bragg reflections, indicative of long-range order, that disappear as the sample is disordered above the T_{ODT}.

is likely not a consequence of spinodal decomposition. This is not surprising since composition fluctuations have been predicted to suppress the spinodal by Frederickson and Helfand.[39]

Since the specific ordered morphologies of these materials have no influence on the RPA spinodal limit of the isotropic phase, we have not yet rigorously characterized them. However, we assert that each specimen does possess long range order at temperatures below T_{ODT} and the transition we observe with DMS is indeed the ODT. This assertion is based on small-angle X-ray scattering (SAXS) experiments that show multiple ordered Bragg reflections below the DMS-located T_{ODT} and a single broad, low intensity peak characteristic of the homogeneous block copolymer melt above T_{ODT}. SAXS intensity vs q profiles for CEE_E-2 and CE_EE-2 appear in Figure 3 and are similar to those obtained for the remainder of the specimens in the study.

Discussion

In this section we compare the experimental behavior of three different ABC and ACB triblock copolymers with the RPA theory: The CEE_E/CE_EE system characterized in the previous section, the SIO/ISO system published by Bailey et al.,[5,40] and the ISD/SID system documented by Hardy et al.[41] We show that there is nearly quantitative agreement between the spinodal T_s-(N, **f**, χ) and equilibrium $T_{ODT}(N$, **f**, χ) surfaces by comparing the two quantities across lines of varying N at fixed **f** (CE_EE/CEE_E) and varying N_O at fixed $N_I =$
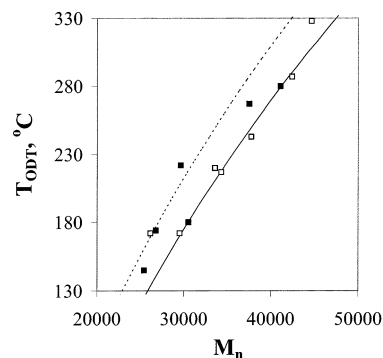

Figure 4. $T_{ODT}(M_n)$ for the CEE_E (□) and CE_EE (■) specimens characterized in Table 2a. T_s calculations are plotted as curves for CEE_E (- -) and CE_EE (—).

N_S (SIO/ISO). Additionally, we compare the scattering behavior of ISD/SID for both SAXS and SANS with the RPA prediction of the structure factor.

The inputs to the RPA calculation are the statistical segment lengths b_i for each monomer type (Table 1), composition **f** (Table 2), degree of polymerization N (Table 2), and the segment−segment interaction parameter χ_{ij} for each polymer pair (Table 3). The interaction parameters used in this study were obtained[33,63−66] by measuring the T_{ODT} in symmetric diblock copolymers and applying the RPA result $\chi N_{ODT} = 10.495$. Reported values of χ have been converted to our choice of monomer reference volume ($v_0 = 118$ Å³) when another value was used in the original study, using the fact that χ is proportional to v_0.

Model CEE_E and CE_EE Triblocks. Figure 4 plots $T_s(M_n)$ and $T_{ODT}(M_n)$ for the CEE_E and CE_EE polymers listed in Table 2, spanning the experimentally observable temperature range. The function $T_{ODT}(M_n)$ is indistinguishable between the two sequences, within the experimental uncertainty in molecular weight and composition. The agreement between the spinodal curves and the experimental data points is excellent, nearly quantitative considering the uncertainty in all of the input parameters to the calculation. The CE_EE T_{ODT} values all lie above the corresponding spinodal curve, as we would expect according to the thermodynamic relationship between the two different quantities, while for CEE_E T_{ODT} is always less than T_s.

In light of the wealth of published examples of the topological dependence of thermodynamic behavior in ABCs,[1,5,40,41] it is at first somewhat surprising that $T_{ODT}(M_n)$ is roughly the same function for both CEE_E and CE_EE, particularly considering the asymmetric relationships among the interaction parameters involved in this system. Throughout the observable temperature range, $\chi_{CE} \gg \chi_{CEE} \approx \chi_{E_EE}$. Since the CE interaction is so large, any ordered CEE_E phase experiences a great deal of enthalpic frustration from the C/E interface. The disordered phase can relieve some of this frustration by dilution of the C/E contacts with the E_E block. Conversely, ordered CE_EE phases can completely exclude C/E contacts; by disordering the system incurs an enthalpic penalty of $k_B T f_C f_E \chi_{CE}$ per chain. All else being equal, one may then surmise that CEE_E would have a lower T_{ODT} value. However, this argument does not account for the importance of the size of the middle block. Consider a set of CE_EE/CEE_E specimens of identical N but with different midblock compositions f_B, with the remainder of the volume distributed evenly among the end blocks. Figure 5 shows the associated
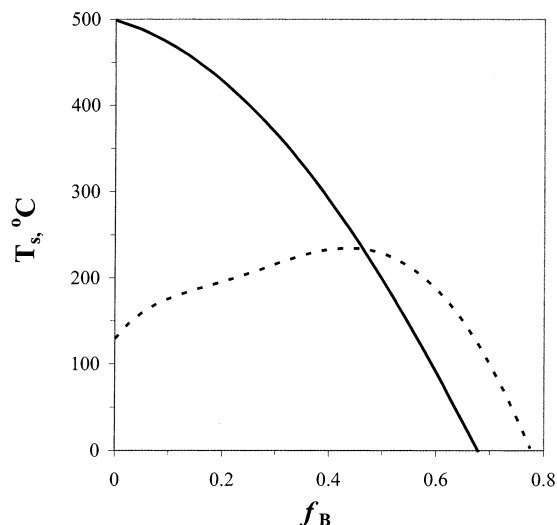
Figure 5. $T_s(f_B)$, where f_B corresponds to the midblock composition in CEE_E (- -) and CE_EE (—), with the remainder of the volume distributed evenly among the end blocks.

RPA prediction, plotting $T_s(f_B)$ for CE_EE and CEE_E with $N = 500$. For small f_B, the C/E contribution to the disordered state free energy has a large influence on the behavior of the two sequences. In CEE_E, this contribution is small because the product f_Cf_E is small. In contrast, the f_Cf_E product is maximized at $f_B = 0$ in CE_EE, and so T_s is greater for this topology at small values of f_B. However, as f_B is increased, the product f_Cf_E decreases monotonically for CE_EE but passes through a maximum in CEE_E. For this reason the two curves intersect at about $f_B = 0.47$, which rationalizes the topological independence of the T_{ODT} observed in the polymers of Figure 4.

Model ISO and SIO Triblocks. The characterization data for SIO/ISO by Bailey et al.[5,40] appear in Table 2. The ISO and SIO series were both constructed by attaching O blocks of various lengths to compositionally symmetric, hydroxyl-terminated SI or IS diblocks. Since a single batch of the SI or IS parent molecule was used to make each series, each SIO/ISO polymer is identical to the others in the series except for the O block length. Figure 6 shows the function $T_{ODT}(N_O)$ for these specimens along with the spinodal curves $T_s(N_O)$, calculated with χ parameters given in Table 3.

The sequence dependence of the ODT is quite strong in this system. T_s and T_{ODT} both monotonically increase as N_O is increased in the ISO sequence while there is a minimum in the SIO sequence. $T_s(N_O)$ matches nearly quantitatively the experimental behavior of both systems, slightly overestimating dT_s/dN_O in both sequences. It is not clear if this is due to limitations in the theory or errors in the interaction parameters used to make the calculations.

In diblock copolymers with upper critical solution temperature behavior the T_{ODT} is strictly an increasing function with respect to N so we might expect the same to be true in ABCs. However, SIO clearly violates this expectation. The initial dip in the T_{ODT} for small O block sizes can be explained by considering the interaction parameters that dictate the thermodynamics of the system, $\chi_{IO} \gg \chi_{SI} \approx \chi_{SO}$. In microphase-separated SIO with sufficiently small O content, the O monomers are dispersed within the I domain rather than segregated into their own domain. Phase separation consequently increases the number of costly I/O contacts in the
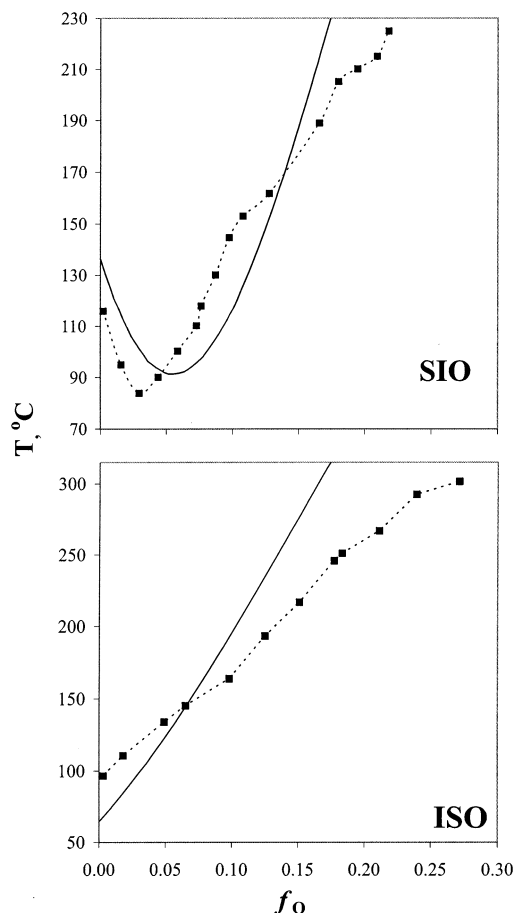

Figure 6. $T_{ODT}(N_O)$ for the SIO and ISO polymers described in Table 2b (points), alongside the RPA spinodal prediction (curves).

ordered phase relative to the disordered phase, where I/O contacts are diluted by S/O contacts. Addition of a sufficiently small O block thus raises the free energy of the ordered phase more than that of the disordered phase, which lowers T_{ODT}. Once the O block is sufficiently large to segregate into its own domain the system can reduce the number of I/O contacts and the disordered state loses its enthalpic advantage, causing T_{ODT} to increase. On the other hand, microphase separation of large I and S blocks in an ISO copolymer with small O block preferentially segregates O into the S-rich region, reducing the number of I/O contacts in the ordered phase relative to that in the disordered phase, and T_{ODT} increases monotonically with increasing O content. It is remarkable that the behavior rationalized by these arguments, which depend on qualitative comparisons of the free energy of the ordered and disordered states, is predicted by the RPA theory without the need to make such comparisons, highlighting the utility of the theory as a predictive tool.

Isotropic Scattering of ISD4 and SID7. Scattering in disordered diblock copolymers has been modeled and curve-fit frequently using Leibler's prediction for the structure factor.[32] In all reported cases, the scattered intensity profile consists of a broad maximum located at a wavevector q^* that corresponds roughly to the most probable length scale between the A and B blocks. In a study recently published by Hardy et al.[41] there appears small-angle X-ray scattering (SAXS) from a disordered, compositionally symmetric ISD triblock copolymer that has two distinct maxima. To our knowledge this behav-
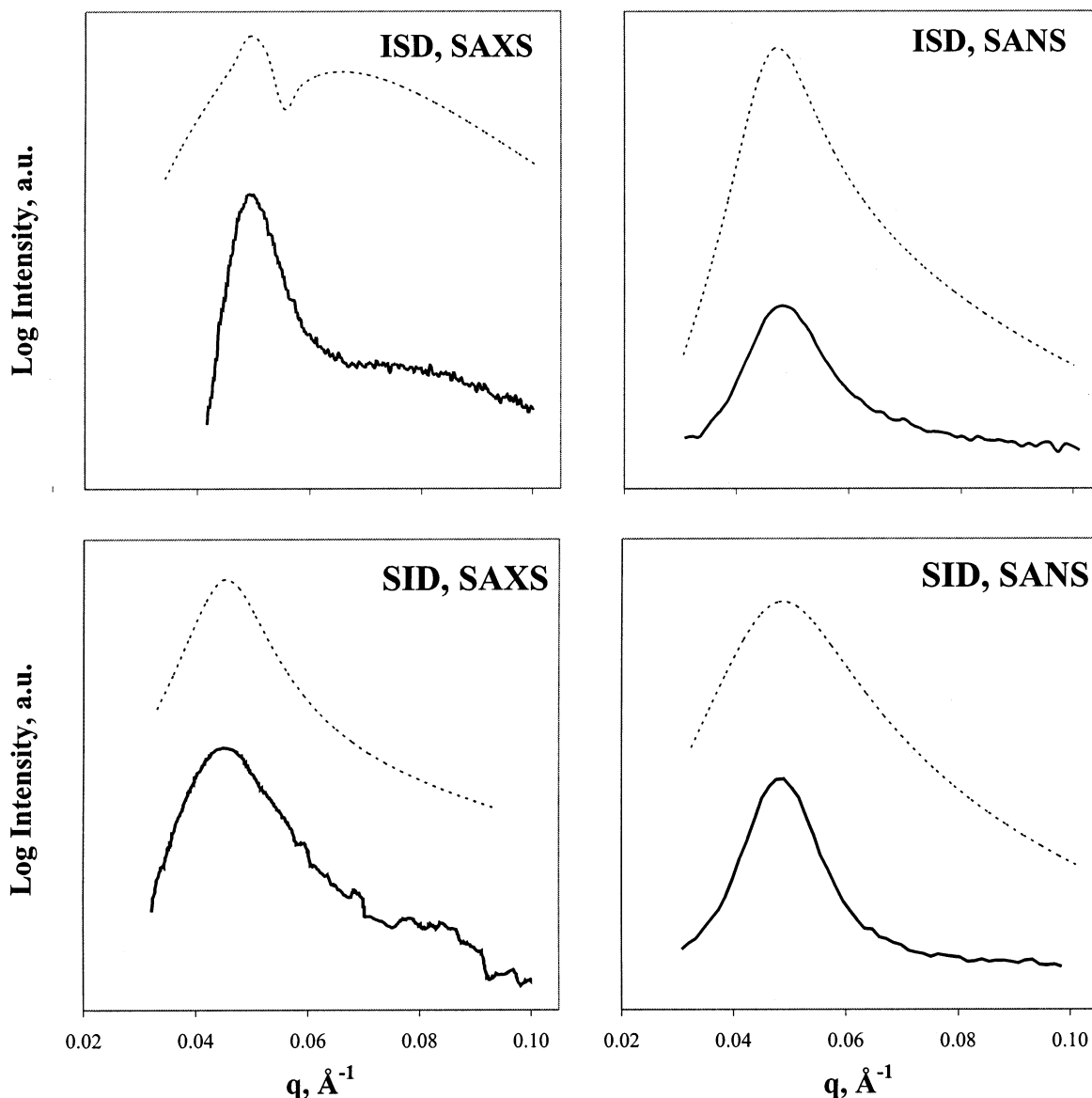
Figure 7. RPA predicted SAXS and SANS profile (dashed curves) for the isotropic phase in ISD4 and SID7, plotted alongside the experimental result (solid curves). The q-axis in the RPA curve has been rescaled by 30% so that the q^* peaks have the same q value as the corresponding experimental data.

ior has not yet been reported elsewhere. However, this second peak appears only in SAXS experiments; small-angle neutron scattering (SANS) on the same specimen yielded a single-peaked scattering profile typical of isotropic diblock copolymer scattering behavior. The presence of the second peak also was sensitive to the block topology, since disordered SID of similar molecular weight and composition to the ISD sample had a single maximum profile in both SAXS and SANS experiments.

We calculated the RPA structure factor for these two specimens, whose characteristics are tabulated in Table 2. The spinodal temperatures were 39 °C and 186 °C for ISD4 and SID7, respectively. The agreement of T_s to T_{ODT} in SID7 is similar in quality to the other examples examined in this study, but that with ISD4 is somewhat disappointing.

Using the scattering length densities in Table 1 the SAXS and SANS behavior for the ISD4 and SID7 were calculated. Figure 7 compares the RPA scattering results at $(T_s + 10)$ °C with the data collected by Hardy et al.[41] at $(T_{ODT} + 10)$ °C. The RPA q values in this figure were compressed to 70% of their predicted value so that

the location of the principal peak maximum q^* matches the experimental value. This rescaling of the q axis is also necessary in order to obtain agreement with the experimentally determined q^* of the polyolefin ABCs of Table 1, and is believed to be a result of the stretching of the copolymer by compositional fluctuations near the ODT,[63] which is not accounted for by the RPA. The location of q^* in the RPA structure factor for triblock copolymers is a function of N, b_i, and χ_{ij}. In triblock copolymers, the value of q^* is sensitive to the interaction parameters. The correlations for the $\chi_{ij}(T)$ in the present study were all obtained by applying the mean-field result $\chi(T_{ODT}) = 10.495/N$ for symmetric diblock copolymers. An alternate method of obtaining $\chi(T)$ is through fitting scattering data from homogeneous blends or diblock copolymers to the mean-field prediction, using $\chi(T)$ as an adjustable parameter. It has been shown by Maurer et al.[67] that these different methods yield entirely different values for the same interaction. It is possible that the mismatch in q^* in the results presented here might arise in part from then using $\chi_{ij}(T)$ measured from diblock T_{ODT} data to predict scattering

behavior. In diblock copolymers the location of $q*$ is independent of χ_{AB}. However, the same 70% rescaling is necessary to make the RPA $q*$ conform to the experimental value measured in the CE diblocks reported in a recent study by the authors.[64] This suggests that there is a failure of the RPA to correctly model the conformational characteristics of the melt near the ODT, not peculiar to these triblock copolymers.

Apart from this inaccuracy, the theoretical structure factor correctly captures the qualitative features of the scattering intensities for these disordered melts. The RPA prediction for X-ray scattering from ISD4 contains two very distinct maxima that are absent when the same structure factor is combined with the neutron scattering lengths. The location of the second peak is approximately $\sqrt{2}q*$ according to both the data and the theory. For SID7, the RPA predicts a single broad peak in both SAXS and SANS that is consistent with the experimental data.

In ABC triblock copolymers, there are potentially three length scales that could be identified in the structure factor through a scattering experiment, corresponding to correlations between the A/B, A/C, and B/C blocks. The $\sqrt{2}q*$ location of the second peak in the ISD4 SAXS data indicates that the second prominent length scale is $1/\sqrt{2}$ the magnitude of the first. This is consistent with the Gaussian scaling of the average distance between two monomers separated by N and $N/2$ repeat units (i.e., $h^2 = Nb^2$), indicating that the two peaks identify midblock−end block (high q) and end block−end block correlations (low q). In Figure 1, in which the RPA scattering was computed for a model compositionally symmetric ISD polymer, the dominant peak was shifted from the first (Figure 1a) to the second (Figure 1b) by merely reducing the contrast between the I and D blocks (i.e. $c_3 − c_1$) roughly 10%, thereby increasing the intensity of the midblock−end block correlations (higher q) with respect to the end block−end block correlations. This comparison shows that the observation of the two length scales in this specimen is strongly dependent on the electron densities. Even a small change in electron density can change the dominant peak or eliminate the second peak altogether. Another influence on the prominence of the midblock−end block correlation is χ_{SD}, which is quite strong with respect to the other interactions in the system. This strong interaction narrows the distribution of length scales between the midblock S and end block D, greatly amplifying the intensity of the second peak. This effect is shown in Figure 8, in which the SAXS behavior is calculated for ISD4 for increasing values of $\chi_{SD}(T)$. A 3% increase in the temperature-dependent term of χ_{SD}-(T) is more than sufficient to make the high-q peak dominant. As χ_{SD} is increased further the second peak sharpens and becomes more dominant until the peak showing end block−end block correlations is completely suppressed.

For the second peak to be present there must be sufficient levels of contrast between all binary pairs. This was also demonstrated with the RPA calculation, in Figure 1c, by matching the contrast of the end blocks, leaving only a single peak representing midblock−end block correlations. In ISD4 there is a strong S/I and S/D contrast that reveals midblock−end block correlations and a weak I/D contrast that shows the correlations between end blocks. In SID7 the distinction between midblock−end block and end block−end block is blurred
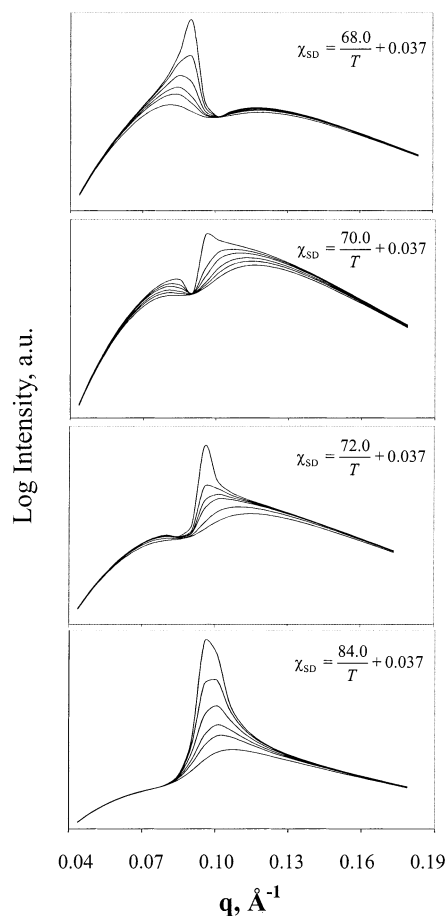

Figure 8. Computed SAXS intensity for ISD4 at temperatures approaching the spinodal for increasing values of χ_{SD}.

because in this case the weak I/D contrast makes the polymer look diblocklike. In neutron scattering, the S/D and S/I contrasts are an order of magnitude larger than the I/D contrast, conforming closely to the case of Figure 1c where the I and D contrast factors are matched. Thus, both ISD4 and SID7 exhibit diblocklike scattering behavior because only the S block is distinguishable with neutrons.

Summary

The RPA theory was applied to the analysis of linear multiblock copolymers. By calculating the RPA structure factor we are able to determine the spinodal stability limit T_s of any block copolymer for which the Flory binary interaction parameters are well-characterized. The spinodal was found to correlate closely to the experimentally observed equilibrium phase transition in four different species of ABC block copolymer.

In the CE$_E$E and CEE$_E$ series, the T_{ODT} was measured as a function of molecular weight at constant composition. For this particular composition, the block topology did not influence the T_{ODT}. The T_s calculation for these two species was in agreement with this finding, matching the experimental temperature dependence and magnitude of the T_{ODT}. The theory was further employed to confirm that the transition was sequence-independent for only a small composition range corresponding to the species under study.

In the SIO and ISO studies of Bailey et al.,[5] the T_{ODT} was measured for varying N_O at fixed $N_S = N_I$. In these experiments, the T_{ODT} of ISO series increased monotonically with N_O while that of the SIO sequence

decreased through a minimum for short O blocks. The reason for this was attributed to the frustration in microphase-separated SIO that exists because of the highly unfavorable I/O interface. This behavior that is justified with equilibrium considerations was also anticipated with the RPA spinodal, indicating that the spinodal limit does indeed lie near the equilibrium transition.

Finally, we demonstrated that the RPA structure factor is representative of the true structure in disordered ABCs by comparing SAXS and SANS data from the compositionally symmetric ISD and SID systems reported by Hardy et al.[41] with the RPA calculation. The theory was able to reproduce the two-peaked $I(q)$ profile observed only in SAXS on ISD. This seemingly anomalous behavior is attributed to the natural existence of multiple length scales in ABCs and the need for an appropriate level of contrast to observe them.

References and Notes

(1) Abetz, V.; Stadler, R. *Macromol. Symp.* **1997**, *113*, 19−26.
(2) Abetz, V.; Stadler, R. T.; Leibler, L. *Polym. Bull. (Berlin)* **1996**, *37*, 135−142.
(3) Abetz, V.; Professorial Dissertation, Bayreuth University, Bayreuth, Germany, 2000.
(4) Auschra, C.; Stadler, R. T. *Macromolecules* **1993**, *26*, 2171−2174.
(5) Bailey, T. S.; Pham, H. D.; Bates, F. S. *Macromolecules* **2001**, *34*, 6994−7008.
(6) Brinkmann, S.; Stadler, R. T.; Thomas, E. L. *Macromolecules* **1998**, *31*, 6566−6572.
(7) Huckstadt, H.; Gopfert, A.; Abetz, V. *Polymer* **2000**, *41*, 9089−9094.
(8) Mogi, Y.; Mori, K.; Kotsuji, H.; Matsushita, Y.; Noda, I.; Han, C. *Macromolecules* **1993**, *26*, 5169−5173.
(9) Mogi, Y.; Nomura, M.; Kotsuji, H.; Onishi, K.; Matsushita, Y.; Noda, I. *Macromolecules* **1994**, *27*, 6755.
(10) Neumann, C.; Loveday, D. R.; Abetz, V.; Stadler, R. T. *Macromolecules* **1998**, *31*, 2493−2500.
(11) Neumann, C.; Abetz, V.; Stadler, R. T. *Colloid Polym. Sci.* **1998**, *276*, 19−27.
(12) Shefelbine, T. A.; Vigilid, M. E.; Matsen, M. W.; Hajduk, D. A.; Hillmyer, M. A.; Cussler, E. L.; Bates, F. S. *J. Am. Chem. Soc.* **1999**, *121*, 8457−8465.
(13) Stadler, R. T.; Auschra, C.; Bechmann, J.; Krappe, U.; Voigt-Martin, I.; Leibler, L. *Macromolecules* **1995**, *28*, 3080−3097.
(14) Matsen, M. W.; Schick, M. *Phys. Rev. Lett.* **1994**, *72*, 2660−2663.
(15) Bates, F. S.; Fredrickson, G. H. *Phys. Today* **1999**, *32*, 32−38.
(16) Khandpur, A. K.; Foerster, S.; Bates, F. S.; Hamley, I. W.; Ryan, A. J.; Bras, W.; Almdal, K.; Mortensen, K. *Macromolecules* **1995**, *28*, 8, 8796−8806.
(17) Matsen, M. W.; Bates, F. S. *J. Chem. Phys.* **1997**, *106*, 2436−2448.
(18) Foerster, S.; Khandpur, A. K.; Zhao, J.; Bates, F. S.; Hamley, I. W.; Ryan, A. J.; W.; B. *Macromolecules* **1994**, *27*, 6922−6935.
(19) Bates, F. S.; Schulz, M. F.; Khandpur, A. K.; Foerster, S.; Rosedale, J. H. *Faraday Discuss.* **1995**, *98*, 7−18.
(20) Hillmyer, M. A.; Bates, F. S.; Almdal, K.; Mortensen, K.; Ryan, A. J.; Fairclough, J. P. A. *Science* **1996**, *271*, 976−978.
(21) Schulz, M. F.; Khandpur, A. K.; Bates, F. S.; Almdal, K.; Mortensen, K.; Hajduk, D. A.; Gruner, S. M. *Macromolecules* **1996**, *29*, 2857−2867.
(22) Odell, J. A.; Keller, A. *Polym. Eng. Sci.* **1977**, *17*, 543−558.
(23) Pakula, T.; Saijo, K.; Kawai, H.; Hashimoto, T. *Macromolecules* **1985**, *18*, 1294−1302.
(24) Koppi, K. A.; Tirrel, M.; Bates, F. S. *Phys. Rev. Lett.* **1993**, *70*, 1449−1452.
(25) Fredrickson, G. H. *J. Rheol.* **1994**, *38*, 1045−1067.
(26) Gupta, V. K.; Krishnanmoorti, R.; Kornfield, J. A.; Smith, S. D. *Macromolecules* **1995**, *28*, 4464−4474.

(27) Patel, S. S.; Larson, R. G. *Macromolecules* **1995**, *28*, 4313−4318.
(28) Hajduk, D. A.; Tepe, T.; Takenouchi, H.; Tirrel, M.; Bates, F. S.; Almdal, K.; Mortensen, K. *J. Chem. Phys.* **1998**, *108*, 326−333.
(29) Fredrickson, G. H.; Ganesan, V.; Drolet, F. *Macromolecules* **2002**, *35*, 16−39.
(30) Bohbot-Raviv, Y.; Wang, Z.-G. *Phys. Rev. Lett.* **2000**, *85*, 3428.
(31) de Gennes, P. G. *J. Phys. (Paris)* **1970**, 235.
(32) Leibler, L. *Macromolecules* **1980**, *13*, 1602−1617.
(33) Maurer, W. W.; Bates, F. S.; Lodge, T. P.; Almdal, K.; Mortensen, K.; Frederickson, G. H. *J. Chem. Phys.* **1998**, *108*, 2989−3000.
(34) Cho, J. *Macromolecules* **2001**, *34*, 1001−1012.
(35) Erukhimovich, I.; Abetz, V.; Stadler, R. T. *Macromolecules* **1997**, *30*, 7435−7443.
(36) Werner, A.; Frederickson, G. H. *J. Polym. Sci., Part B: Polym. Phys.* **1997**, *35*, 849−864.
(37) Akcasu, A. Z.; Klein, R.; Hammouda, B. *Macromolecules* **1993**, *26*, 4136−4143.
(38) Brazovskii, S. A. *Zh. Eksp. Teor. Fiz.* **1975**, *68*, 195.
(39) Fredrickson, G. H.; Helfand, E. *J. Chem. Phys.* **1987**, *87*, 697−705.
(40) Bailey, T. S.; Hardy, C. M.; Epps, T. H., III.; Bates, F. S. *Macromolecules* **2002**, *35*, 7007−7017.
(41) Hardy, C. M.; Bates, F. S.; Kim, M.-H.; Wignall, G. D. *Macromolecules* **2002**, *35*, 3189−3197.
(42) Vilgis, T. A.; Benmouna, M.; Benoit, H. *Macromolecules* **1991**, *24*, 4481−4488.
(43) Benmouna, M.; Benoit, H.; Borsali, R.; Duval, M. *Macromolecules* **1987**, *20*, 2620−2624.
(44) Akcasu, A. Z.; Benmouna, M.; Benoit, H. *Polymer* **1986**, *27*, 1935−1942.
(45) Benoit, H.; Benmouna, M. *Polymer* **1984**, *25*, 1059−1067.
(46) Akcasu, A. Z.; Tombakoglu, M. *Macromolecules* **1990**, *23*, 607−612.
(47) Benoît, H.; Benmouna, M.; Wu, W.-l. *Macromolecules* **1990**, *23*, 1511−1517.
(48) Ndoni, S.; Papadakis, C. M.; Bates, F. S.; Almdal, K. *Rev. Sci. Instrum.* **1995**, *66*, 1090−1095.
(49) Gilman, H.; Cartledge, F. K. *J. Organomet. Chem.* **1964**, *2*, 447−454.
(50) Jones, T. Ph.D. Thesis, University of Minnesota, Minneapolis, MN, 2000.
(51) Gehlsen, M. D. Ph.D. Thesis, University of Minnesota, Minneapolis, MN, 1993.
(52) Bates, F. S.; Fredrickson, G. H.; Hucul, D.; Hahn, S. F. *AIChE J.* **2001**, *47*, 762−765.
(53) U.S. Patent 5,612, 422.
(54) U.S. Patent 6,090, 359.
(55) Fetters, L. J.; Lohse, D. J.; Richter, D.; Witten, T. A.; Zirkel, A. *Macromolecules* **1994**, *27*, 4639−4646.
(56) Rosedale, J. H.; Bates, F. S. *Macromolecules* **1990**, *23*, 2329−2338.
(57) Gehlsen, M. D.; Almdal, K.; Bates, F. S. *Macromolecules* **1992**, *25*, 939−943.
(58) Bates, F. S.; Rosedale, J. H.; Fredrickson, G. H. *J. Chem. Phys.* **1990**, *92*, 6255−6270.
(59) Hashimoto, T.; Sakamoto, N.; Koga, T. *Phys. Rev. E: Stat. Phys., Plasmas, Fluids, Relat. Interdisc. Top.* **1996**, *54*, 5832−5835.
(60) Koga, T.; Koga, T.; Hashimoto, T. *Phys. Rev. E: Stat. Phys., Plasmas, Fluids, Relat. Interdisc. Top.* **1999**, *60*, R1154−R1157.
(61) Kim, W. G.; Garetz, B. A.; Newstein, M. C.; Balsara, N. P. *J. Polym. Sci., Part B: Polym. Phys.* **2001**, *39*, 2231−2242.
(62) Balsara, N. P.; Garetz, B. A.; Newstein, M. C.; Bauer, B. J.; Prosa, T. J. *Macromolecules* **1998**, *31*, 7668−7675.
(63) Rosedale, J. H.; Bates, F. S.; Almdal, K.; Mortensen, K.; Wignall, G. D. *Macromolecules* **1995**, *28*, 1429−1443.
(64) Cochran, E. W.; Bates, F. S. *Macromolecules* **2002**, *35*, 7368−7374.
(65) Hashimoto, T.; Ijichi, Y.; Fetters, L. J. *J. Chem. Phys.* **1988**, *89*, 2463−2472.
(66) Almdal, K. Personal communication, 2002.
(67) Maurer, W. W.; Bates, F. S.; Lodge, T. P.; Almdal, K.; Mortensen, K.; Fredrickson, G. H. *J. Chem. Phys.* **1998**, *108*, 2989−3000.